Wavefront engineering to enhance atom-light interaction

Chow Chang Hoong

an academic exercise presented in partial fulfillment for the

degree of Bachelor of Science with Honours in Physics

Supervisor: Professor Christian Kurtsiefer

Department of Physics

National University of Singapore

2018

ACKNOWLEDGEMENTS

I would like to express my greatest gratitude to my supervisor Professor Christian Kurtsiefer for the opportunity to work in this project.

My sincere thanks to Matthias who has been extremely patient in giving me guidance for the project and refining my understandings. Many times he babysitted me to complete the painful infinite loop of tuning mirrors and performing knife-edge measurements.

I would also like to thank Wilson for all the encouragements and discussions. He pampered me with lab basics when I was still struggling with fiber coupling, not to mention that he also went through the pain of reading the first draft of this thesis.

To Xi Jie, thank you for the good times when we worked together like a Swiss clock, for all the free food information as well as the anime talks.

To everyone else in the lab and friends, thank you for the exciting year!

Abstract

We aim to use a spatial light modulator to minimize the focal spot size of a laser beam by pre-correcting the optical aberrations. The beam waist radius, taken as a figure of merit, is measured using the knife-edge method before and after the optimization. In this thesis, we report on the setting up of lenses and a razor blade mounted onto a piezo-driven stage to measured the beam waist radius. Optimization algorithm based on Zernike polynomials manages to reduce the waist radius. The reconstruction of beam profiles shows that the light intensity increases at the end of optimization, which confirms that the focusing is improved.

Contents

1   Introduction

Atom-light interaction has received a considerable amount of interest in recent years for its essential role in different quantum communication and computation protocols [1]. One of the major stumbling blocks in these protocols lies in achieving efficient transfer of quantum information from a photonic qubit to an atomic qubit.

The canonical approach to increase the interaction strength of an atom with incoming light is to place a high-finesse cavity around the atom [2, 3]. By having a large cavity finesse or a small mode volume, the electrical field strength of a single photon is greatly enhanced by multiple reflections between two highly reflective mirrors, resulting in a high atom-field coupling strength. Although this method has seen tremendous success over the years, working with such cavities is still a technological challenge. Most cavity quantum electrodynamics experiments in the optical domain are employing cavities based on delicate dielectric coatings which are technically hard to fabricate [4]. Besides, there are also challenges in stabilizing the cavities against vibrations, which makes it experimentally difficult to scale up such schemes to the desired quantum networks.

An alternative approach is to consider an atom-light interface in free-space in which the atom interacts with the full continuum of field mode spectrum. The concept of this technique is simply to strongly couple a single atom to incoming light field with the help of a large numerical aperture (NA) lens [5]. Motivated by the fact that the absorption cross section of an atom is of the order of the square of the optical wavelength, which is close to a diffraction limited spot size of a focusing lens, studies are well under way [6]. A recent theoretical research on this matter predicts that it is possible to reach deterministic absorption of single photons for dedicated focusing geometries [7].

In the majority of the experiments, interaction strength is characterized by

Table 1: State of the art of coupling single atoms and photons in free space.

Experimental system	Year	Extinction	Coupling efficiency
Trapped ion [9]	1987	$\leq 0.1\%$	
Quantum dot [11]	2007	12%	
Molecule in matrix [10]	2008	22%	
Trapped atom [15]	2008	10%	
Trapped ion (parabolic mirror) [13]	2014		7.2%
Trapped atom [12]	2017	36.6%	
Trapped ion (parabolic mirror) [14]	2017		13.7%

transmission measurements. The total field measured is a superposition of the recollimated incident field and the field scattered by the atom. There is a phase difference between these two fields; hence we will see destructive interference which leads to an extinction of the beam. For a numerical aperture of one (focusing from half solid angle) and an incoming field resembling dipole radiation, complete extinction in the forward direction is predicted [8]. Some of the important milestones of extinction measurements are recorded in Table 1. The first transmission spectrum of a single atom was observed for a ^{198}Hg+ ion. The absorption probability of the probe photons in that experiment was estimated to be about 2.5×10^{-5} [9]. Recently performed experiments on single molecules and semiconductor quantum dots reported a signal contrast up to 22% [10, 11]. Substantial attenuation of the forward traveling beam has been reported occasionally, the maximum extinction achieved was about a factor of 5 below the optimum value, until an experiment in which the focusing optics covers most of the solid angle (adapting from 4π microscopy technique) demonstrates an extinction of around 36.6% [12]. Similarly, exceptionally high coupling efficient of a trapped ^{174}Yb+ ion and light focused with parabolic mirrors are reported when illuminating with from half and nearly full solid angle [13, 14].

In connection with the absorption of single photons, the crucial role of the

solid angle has been highlighted above. However, the interaction strengths observed with these configurations have fallen short of their theoretically expected capabilities. It has been suspected that the thermal motion of atom in free space could be a limiting factor for atom-light interaction. A study has shown that only a moderate improvement of interaction strength is promised by cooling to the motional ground state of atom [16]. We are also limited by the imperfections of optical elements in the experiment. In general, the efficiency of photon absorption is proportional to the extent to which the incoming light mode resembles an electric dipole wave. However, the real lenses are not ideal lenses; as a consequence, the aberrations of the focusing optics lead to distorted spherical wavefront, spread out foci and weak atom-light interaction.

The general strategy is to analyze the focusing lens and to apply aberration corrections to the incoming beam. Since the beam profile at the focal point is studied using the knife-edge method, we do not load atom between the aspheric lenses. A scheme for correcting the aberrations based on beam waist measurement is applied using a spatial light modulator (SLM). A control algorithm is employed to obtain a spatial phase pattern that can minimize the beam waist near focus. The beam profile at the end of optimization is carefully studied.

This thesis is organized as follows. In Section 2, the model used to describe laser beam is given. In Section 3, we present the measurement of beam waist radius using the knife-edge technique. Our experimental setup is also discussed, including the waist radius and M^2 factor that we obtained at the focus for different incident beam waists. In Section 4, we discuss how wavefront aberrations are being corrected. Results of our optimization scheme are also shown. Finally, Section 5 contains summarizing remarks.

2 Paraxial Gaussian Beam Model

We describe the Gaussian beam model used in our experiment. The passage of the Gaussian beam through a perfect lens and the approximations applied are also discussed. Particularly, we obtain the beam waist radius at the focal point as a function of incident beam waist radius.

2.1 Propagation of Gaussian Beams

In the heart of our study, we consider a linearly polarized, monochromatic, radially symmetric Gaussian laser beam with electric field described by

$$\vec{E}(r, z) = \vec{E}_0 \frac{w_0}{w(z)} \exp\left(-\frac{r^2}{w(z)^2}\right) \exp\left(-i\left(kz + k\frac{r^2}{2R(z)}\right)\right), \tag{1}$$

where r and z represent the radial and axial component from the beam in cylindrical coordinate; k is the wave number; $w(z)$ is the beam radius at position z, defined as the radius at which the electric field amplitudes drop to $1/e$ of its axial value; w_0 represents the waist radius; $R(z)$ is the radius of curvature of the beam's wavefront at position z.

The variation of beam radius $w(z)$ along the propagation direction is given by

$$w(z) = w_0\sqrt{1 + \left(\frac{z - z_0}{z_R}\right)^2}, \tag{2}$$

with the Rayleigh length $z_R = \frac{\pi w_0^2}{\lambda}$ where λ denotes the wavelength of laser beam. z_0 is the location where the beam radius is at its minimum. The evolution of radius of curvature $R(z)$ is given by

$$R(z) = (z - z_0)\left[1 + \left(\frac{z_R}{z - z_0}\right)^2\right]. \tag{3}$$

4

One can see that the geometric dependence of a Gaussian beam's electric field is governed by $w(z)$ and $R(z)$, which are both functions of position $(z - z_0)$ and Rayleigh length z_R (or waist radius w_0).

2.2 Focusing with Lenses

For the purpose of our study, we suppose that the Gaussian beam traverses a perfect lens with focal length f, i.e., we assume the lens is aberration free and not affected by the aperture size. When the propagation direction of light deviates only slightly from the optical axis, the light path can be expressed with only the lowest order terms of divergence angle. This small angle approximation is the paraxial approximation. We work with low to moderate focusing in the experiment, which is the regime where parabolic approximation still holds. Hence, the change in electric field after passing through a lens is denoted by

$$\vec{E'} = e^{ikr^2/2f}\vec{E}, \tag{4}$$

where $\vec{E'}$ is the electric field immediately after a lens. Here we use prime to represent electric field properties in the image space. One important feature of $\vec{E'}$ is that it remains Gaussian, with $w' = w$ and $\frac{1}{R'} = \frac{1}{R} - \frac{1}{f}$ where w' and R' are the beam radius and the radius of curvature right after the lens; w and R are the beam radius and the radius of curvature right before the lens.

The beam radius is at its minimum near the focus. By manipulating Eq. 2 we are able to relate beam waist at the lens w_{in} and beam waist at the focus w_0:

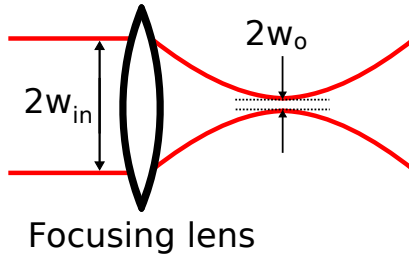$$w_{in} = w_0\sqrt{1 + (\frac{f\lambda}{\pi w_0^2})^2}.$$

Figure 1: Gaussian beam passing through a lens. w_{in}: waist radius right before the lens. w_0: waist radius at the focal point. The two radii are related by Eq. 5

Near the focus, w_0 and λ are on the same order while $f \gg w_0$. The expression above can be further simplified, which gives

$$w_{in} \simeq \frac{f\lambda}{\pi w_0}.$$

(5)

One has to take note that polarization is not taken into account in previous derivations. In fact, the electric field was treated as a scalar field. In the concrete example of a beam which is initially linearly polarized, immediately after the lens, the polarization needs to be modified since each ray has a focusing radial component. As light with different polarizations does not simply add up, a vectorial focusing theory is required. Nevertheless, studies show that the beam is elongated in the polarization direction and we measure beam waist in the same direction in the experiment to not underestimate beam size [17].

3 Knife-edge Measurement

In this section, we describe the scanning knife-edge technique that is used to measure the waist radius of light beam. The experimental arrangement is also shown. We vary the input beam waist radii and measure the resulting focused beam waist at the focal point.

3.1 Basics of Knife-edge

There are several methods for beam characterization, including the knife-edge, point scan, convolution scan and slit. Both point scan and convolution scan require fluorescence labeled latex beads and fluorescent sheets which are not adaptable to the automated waist optimization experiment [18]. For the slit method, the beam is probed with a small slit of width Δ. The Gaussian profile is constructed from the amount of light transmitted through the small slit. This method requires the slit width to be a factor of 20 smaller than the waist radius, which is practically too small for our experiment ($\Delta \simeq 40$nm) [19]. Here we have decided to use the knife-edge scanning technique, which is a well known process that is capable of performing submicron waist measurements [20].

The operation principle of this method is based on an opaque knife-pad or razor-blade which is line-scanned through the transverse cross-section of a beam under study. While scanning, the power of the transmitted light beam that is not blocked by the knife-pad is recorded by a detector. The beam profile can be tomographically reconstructed from the photo-current curves resulting from scans

performed under different directions. The transmitted power is

$$P_z(x) = \frac{\epsilon_0}{2} \int_{-\infty}^{x} \int_{-\infty}^{\infty} |\vec{E}|^2 dx' dy'$$

$$= P_0 \left\{ \frac{1}{2} + \frac{1}{2} \text{ erf}\left[\frac{\sqrt{2}(x - x_0)}{w(z)}\right] \right\}. \tag{6}$$
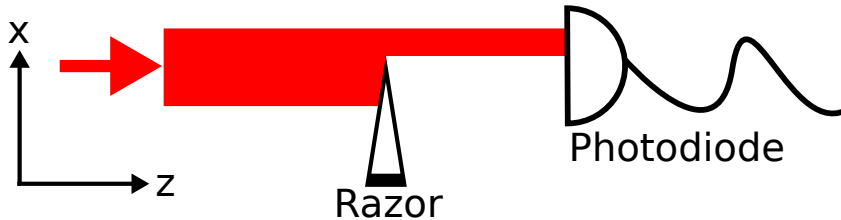

Figure 2: Simplified scheme for the measurement of laser beam radius using the knife-edge technique. The shadow caused by the razor is left blank. x-axis: perpendicular to propagation direction. z-axis: along beam propagation direction.

In experiment, even if the razor blade completely blocks the beam, the photodiode still measures a small background signal. Hence, we modify the previous equation (Eq. 6) to

$$P(x) = P_0 \left\{ \frac{1}{2} + \frac{1}{2} \text{ erf}\left[\frac{\sqrt{2}(x - x_0)}{w_z}\right] \right\} + C_p, \tag{7}$$

where C_p is a constant that can be predetermined when no light goes through.

3.2   Experimental Setup

The schematic diagram of our optical setup is shown in Figure 3. The heart of our setup consists of two identical aspheric lenses of NA = 0.55, f = 4.51 mm (Thorlabs C230) mounted in a confocal arrangement. The linearly polarized Gaussian laser beam is focused by the first lens (test lens) then fully collected by the second lens (collimating lens). We choose to work with 780nm laser because

8

this wavelength drives the closed transition between $5^2\mathrm{S}_{1/2}$, F=2, $\mathrm{m}_F = -2$ and $5^2\mathrm{P}_{3/2}$, F=3, $\mathrm{m}_F = -3$ of $^{87}\mathrm{Rb}$. A sharp razor blade, mounted onto a piezo-driven motorized translation stage (P-611.3 NanoCube PI XYZ Piezo Stage) is placed near the focus to block the beam partially. The blade moves transversely in the focal place (x-direction) to cut the beam, and along the beam propagation direction (z- direction). The transmitted light is detected behind the lenses using a p-i-n photodiode (Hamamatsu S5107).
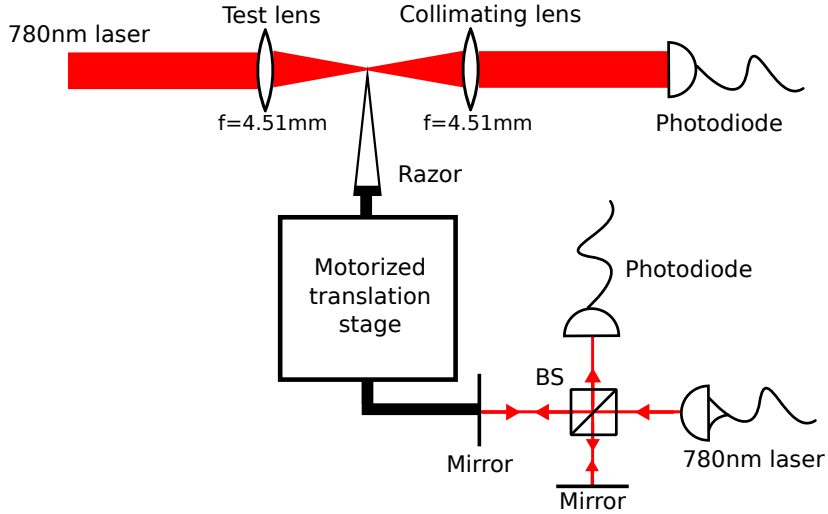
Figure 3: Schematic depiction of the knife-edge technique. A photodiode measures the transmitted beam cut by a razor blade. The position of the blade is calibrated using an interferometer. BS: Beamsplitter.

3.3 Waist Measurement

To extract beam waist parameter with the knife-edge method, the change in transmitted power of the laser beam is measured as the razor is being scanned across the beam. Each of such single knife-edge cut is scanned across a 10.6μm range at intervals of 0.75μm along x-direction. The beam size is then determined by fitting the calibrated data with the modified transmitted power error function (Eq. 7). An example is illustrated in Figure 5. Approximately 30 of these single
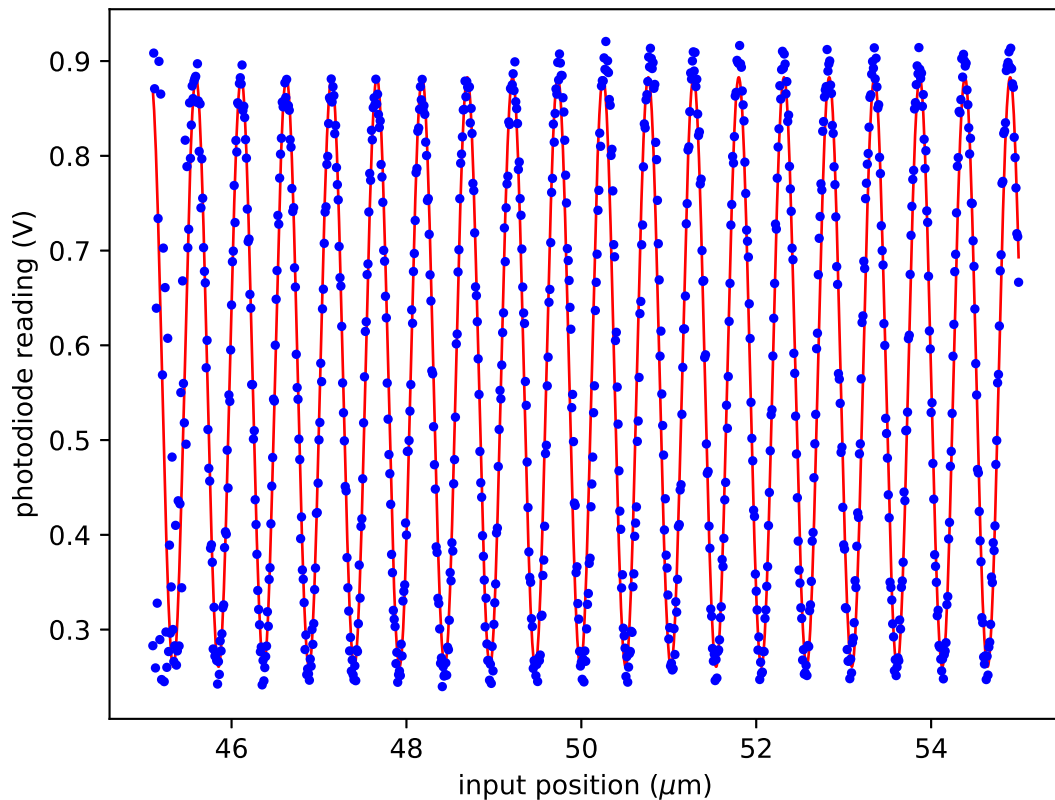
Figure 4: Typical interferometer fringes data for a single knife-edge cut along x-direction. The best fit gives $\alpha = 0.754 \pm 0.003$. Blue dots: data measured by a photodiode, red line: fit to Eq. 9.

x-directional cuts are recorded at intervals of 0.23μm along the beam propagation direction centered around the focal point. To obtain the minimum beam waist, the waist measurements from each of these cuts have to be fitted with Eq. 2. However, real laser beams are not ideal Gaussian beams. To account for the beam divergence led by the non-Gaussian modes, the beam quality factor M^2 needs to be introduced. One modifies the waist evolution (Eq. 2):
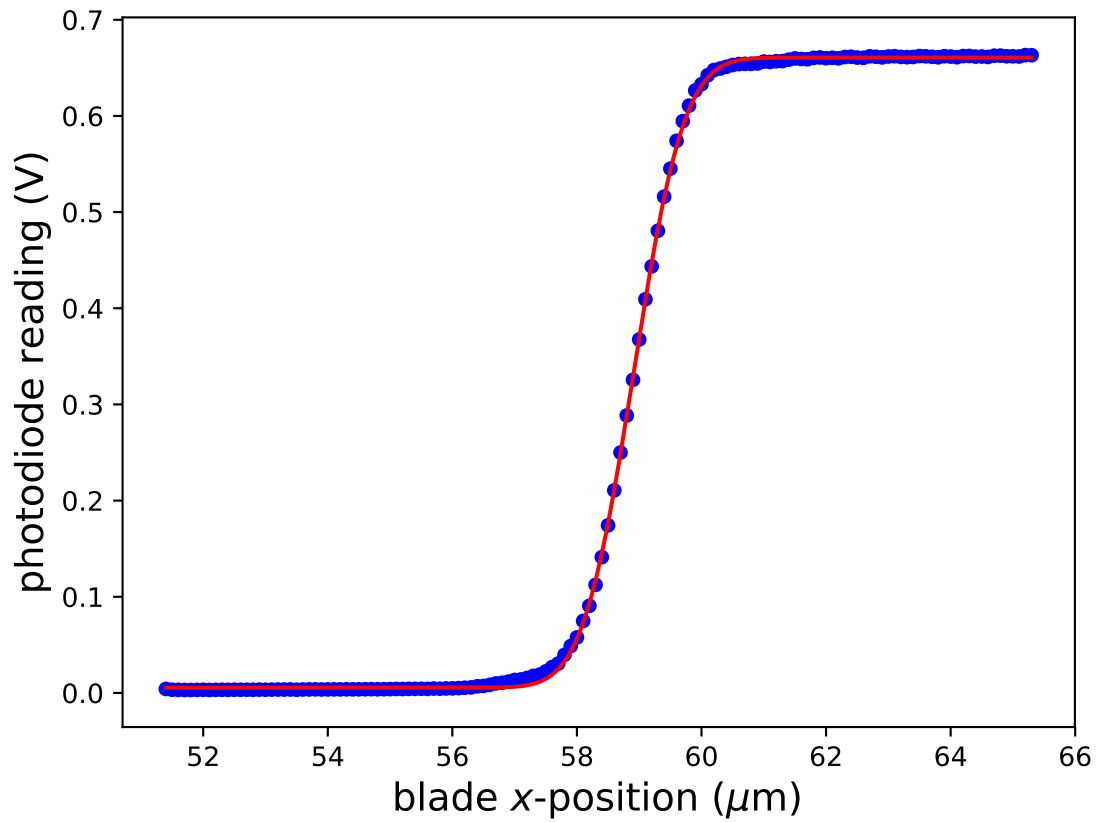
$$w(z) = w_0\sqrt{1 + (\frac{z - z_0}{z_R}M^2)^2}. \tag{8}$$

Figure 5: Typical knife-edge data for a single knife-edge cut along x-direction, the best fit gives $w = 1.28 \pm 0.01\mu$m. Blue dots: data measured by a photodiode, red line: fit to error function (Eq. 7).

The M^2 term here is defined as the ratio of measured and ideal beam divergences. For a perfect Gaussian beam, $M^2 = 1$. Physical beams generally have $M^2 > 1$. One of such fit is shown in Figure 6.

At the early stage of the experiment, the beam waist radius measured using the knife-edge method was always two to three times larger than the theoretical prediction for an ideal Gaussian beam. M^2 measured was consistently smaller than 1, approximately 0.7. We found out that it was due to the PI piezo stage not moving the razor at the right scale. Thus, The position of razor blade is calibrated using an interferometer. Along with the razor blade, a mirror is attached to the opposite side of the translation stage. The mirror plays the role as a reflector for one of the interferometer arms which provides an accurate position calibration of the blade in the direction perpendicular to the beam, as shown in Figure 3.

The photodiode reading is recorded as the razor is being scanned across the beam and is fitted with

$$V(\tilde{x}) = A + B \, \cos(\frac{2\pi}{\lambda} 2\alpha\tilde{x} + \phi), \tag{9}$$

where $\tilde{x}$ is the input position. A, B, α and ϕ are fitting parameters. α is the calibration factor that gives the real position $\alpha\tilde{x}$. The same calibration is also conducted along the z-direction.

3.4 Setting up Telescopes

We would like to examine the field near the focus for different focusing parameters u, defined as
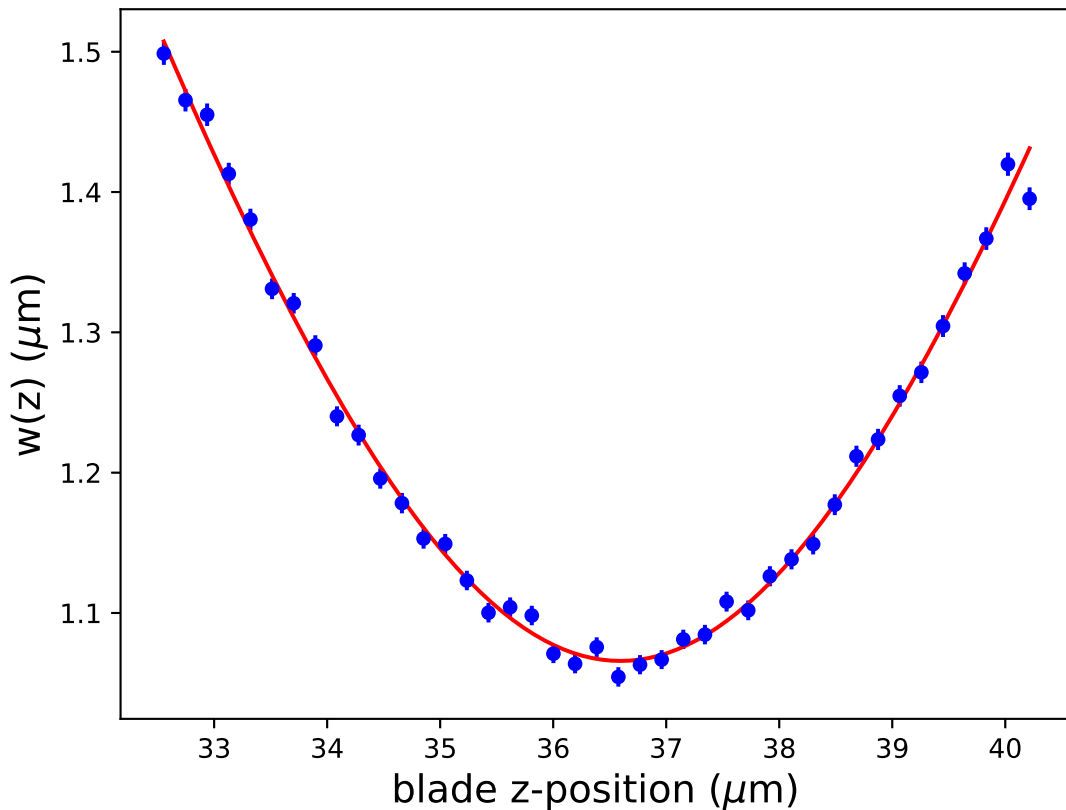
$$u = \frac{w_{in}}{f}. \tag{10}$$

Figure 6: Beam radius near focal point, the best fit gives the waist radius and M^2, which are determined to be $w = 1.066 \pm 0.002\mu$m and $M^2 = 1.133 \pm 0.006$. Blue dots: fitted waist along x-direction, red line: fit to waist evolution (Eq. 8). Error bars represent one standard deviation of propagated fitting uncertainties.

For this, we have chosen different input waists while keeping the focal length of test lens $f = 4.51$mm fixed.

A schematic outline of our experiment is shown in Figure 7. A laser beam is delivered from single mode fiber and collimated with a triplet fiber optic coupler (Thorlabs TC18FC-780) which outputs a beam with waist radius of 1.96mm. To manipulate the input waists, a telescope consisting of two planoconvex lenses with focal lengths f_1 and f_2 in confocal arrangement is placed before the aspheric lenses to (de-)magnify our beam. The four settings that were used in the experiment
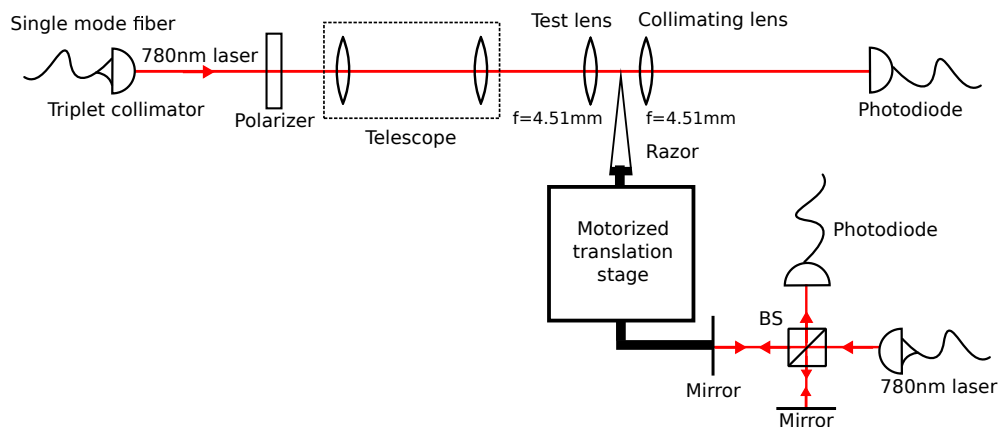
Figure 7: Schematic depiction of the knife-edge measurement with a telescope introduced. The magnification of the telescope decides the incident beam waist.

Table 2: Details of the initial settings in our experiment.

Telescope setting	Magnification	w_{in} (mm)	u	w_f (μm)	Clipping (%)
$f_1 = 100$mm, $f_2 = 50$mm	0.5	0.98	0.217	1.14	10^{-4}
$f_1 = 125$mm, $f_2 = 75$mm	0.6	1.18	0.261	0.95	0.01
$f_1 = 100$mm, $f_2 = 75$mm	0.75	1.47	0.326	0.76	0.26
$f_1 = 100$mm, $f_2 = 100$mm	1.0	1.96	0.435	0.57	3.5

are summarized in Table 2.

Due to finite clear aperture (CA), the beam profile at the focal point is no longer a Gaussian, but a convolution of Airy pattern and Gaussian. The aperture effect is more severe if the beam radius is close to aperture size; and it is characterized by clipping, defined as $\int_{R_{ap}}^{\infty} |\vec{E}(r)|^2 2\pi r dr / \int_0^{\infty} |\vec{E}(r)|^2 2\pi r dr$ (fraction of power blocked by the aperture), where R_{ap} is the aperture radius. For beam sizes in this experiment, the clipping due to finite CA of lens is low. It is also summarized in Table 2.

To obtain a flat wavefront right before the test lens, we autocollimate the beam: one lens of the telescope is attached on a translation stage that moves along the beam propagation direction. A mirror is placed right before the aspheric lenses in order to back-couple the beam into single mode fiber. The amount of light being

14

back-coupled into the fiber is measured with a photodiode and the telescope length is adjusted such that the confocal arrangement maximizes the back-coupling. The tip and tilt of the two mirrors which deliver the beam through the aspheres are also tuned to maximize goodness of error function fit as well as to minimize M^2.

Figure 8 shows the measured waist radius and M^2 for four focusing parameters (different input waist) using knife-edge method. In general, the measured waist radii are larger than those predicted using paraxial Gaussian model, especially for a larger focusing parameter u. We also see that M^2 becomes larger as focusing parameter u increases. There are a few possible reasons for this behavior. First, as the input waist gets larger, it becomes more comparable with the clear aperture of test lens ($2R_{CA} = 5.07$ mm). From Table 2 we can see that there are significant clippings when focusing parameter u is greater than 0.3; hence, we can expect the beam to be less Gaussian for larger focusing parameters. Besides, the beam can also be distorted by aberrations present in the optical system. The setup contains many elements, none of which are perfect. These deformations of optical elements cause aberrations in the beam. It is of our interest to study if the waist radius can be further reduced if the aberrations are corrected.
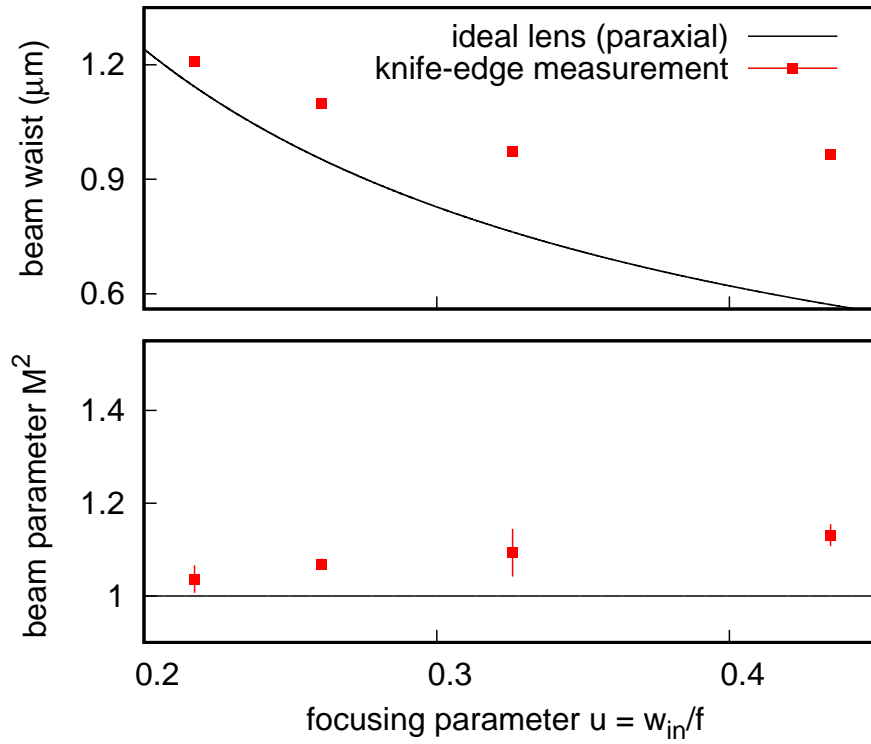
Figure 8: Waist radius and M^2 as a function of focusing parameter u. Red dots: data measured with the knife-edge technique. Black solid line: theoretical results for a paraxial ideal Gaussian beam. Error bars represent one standard deviation of 10 repeated measurements. Error bars in top panel are smaller than symbol size.

4 Waist Optimization

We aim to minimize the focal spot size by pre-correcting the optical aberrations using as spatial light modulator (SLM). To this end, we vary the spatial phase pattern on he SLM and measure the beam waist using the knife-edge method.

4.1 Spatial Light Modulator

In this section, we introduce a device, called a spatial light modulator (SLM) which can alter the phase of laser beam spatially, and use it to pre-correct the aberrations of the optical system. In our experiment, we use a LCD-based reflection spatial light modulator (SLM) from Meadowlark Optics XY P512L series. On the SLM, there are $512 \times 512 = 262144$ active pixels. Each pixel can modify phase up to 2π. Before any additional phase is applied to the SLM, it functions like a mirror. To modify the phase, the polarization of the input beam must be linear and horizontal relative to the SLM. We use a polarizer to ensure the corect polarization of the light. Hence, the SLM must be introduced after a polarizer, as illustrated in Figure 9

To describe the phase pattern uploaded to the SLM, we introduce the set of Zernike polynomials. The phase pattern is expanded in terms of Zernike polynomials.
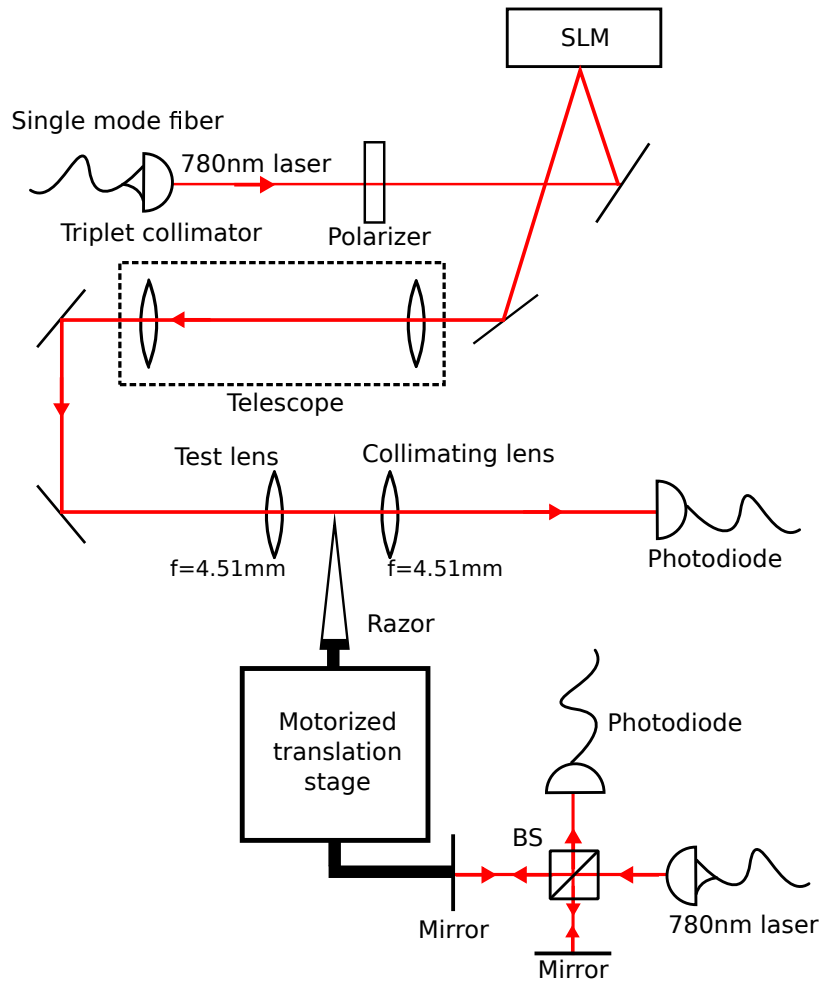
Figure 9: Schematic depiction of the knife-edge measurement with a SLM introduced. A phase pattern is uploaded to the SLM to pre-correct the wavefront errors. BS: Beamsplitter. SLM: Spatial light modulator.

4.2   Zernike Polynomials

Mathematically, the Zernike polynomials (or Zernike modes) form a basis of polynomials that are orthogonal on a unit disk. By definition, each of these Zernike modes is represented with two integer numbers $\{n, m\}$. There are two classes of Zernike modes: even and odd. We can write the even modes as Z_n^m and the odd modes as Z_n^{-m}; in polar coordinate, their expression is given by
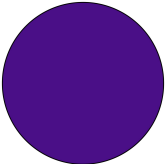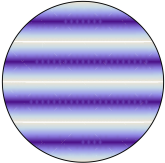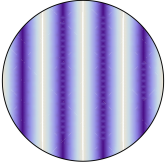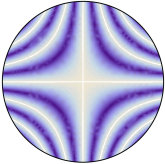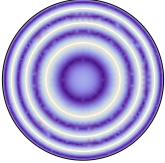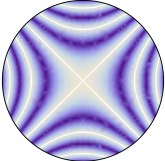
$$
\begin{aligned}
Z_n^m(\rho, \phi) &= R_n^m(\rho)\cos(m\phi), \text{ (even modes)} \\
Z_n^{-m}(\rho, \phi) &= R_n^m(\rho)\sin(m\phi), \text{ (odd modes)} \\
R_n^m(\rho) &= \sum_{k=0}^{\frac{n-m}{2}} \frac{(-1)^k (n-k)!}{k!(\frac{n+m}{2}-k)!(\frac{n-m}{2}-k)!} \rho^{n-2k},
\end{aligned}
\tag{11}
$$

where n, m are nonnegative integer, $n \geq m$ and $m = n, n-2, n-4, \dots$ ($n-m$ must be even). In this experiment, we convert the two indices n and m to a single-index mode number j to facilitate the enumeration. The relation is given by

$$
j = 1 + \frac{n(n+2) + m}{2}.
$$

In general, the polynomials are a standard basis for the description of optical aberrations with the various terms of Zernike expansion corresponding to common aberrations and misalignment such as tip, tilt, defocus, astigmatism, coma and spherical aberrations [21, 22]. Table 3 contains information about the first six Zernike modes.

Table 3: First six Zernike modes. The colour of phase pattern represents a phase of 0 (blue) to π (white).

Mode number j	$\{n,m\}$ indices	Polynomial	Aberration type	Phase visualization
1	$\{0,0\}$	1	Piston	
2	$\{1,-1\}$	$2\rho\,\sin\phi$	Vertical Tilt	
3	$\{1,1\}$	$2\rho\,\cos\phi$	Horizontal Tilt	
4	$\{2,-2\}$	$\sqrt{6}\rho^2\,\sin2\phi$	Oblique Astigmatism	
5	$\{2,0\}$	$3(2\rho^2-1)$	Defocus	
6	$\{2,2\}$	$\sqrt{6}\rho^2\,\cos2\phi$	Vertical Astigmatism	

4.3   Gradient Search Algorithm

The additional phase mask applied to the SLM Φ can be expressed as a linear combination of different Zernike terms:

$$\Phi = \sum_{i=1}^{N} a_i Z_i, \tag{12}$$

where a_i is the weight of i-th Zernike mode. Since it is practically impossible to go through countably infinite number of Zernike expansions, the search space is restricted to encompass N terms.

Waist minimization is an optimization problem; we are looking for the optimal weights of each of the Zernike terms given by

$$\arg \min_{\{a_i\}_{i=1}^{N}} w(\Phi).$$

We have performed a gradient search algorithm in which the weights of Zernike modes are varied one at a time to find a solution. The scheme can be summarized as follows: without any additional phase being applied, SLM plays the role of a flat mirror. A knife-edge measurement is performed (a full measurement includes $n_x = 9$ single knife-edge cuts along x-direction (perpendicular to optical axis) at different z position along the propagation direction), the minimum waist radius is recorded. After initialization, the weight is varied one by one starting from mode $i = 1$ with a weight step size Δa of ± 0.2 (1 corresponds to 2π phase), for each new weight the waist is measured and recorded along with the best weights. The next iteration is based on the best weights of previous iterations. When the search reaches the last mode $i = N$, the following iteration starts from mode $i = 1$ again. The algorithm completes after two full cycles.
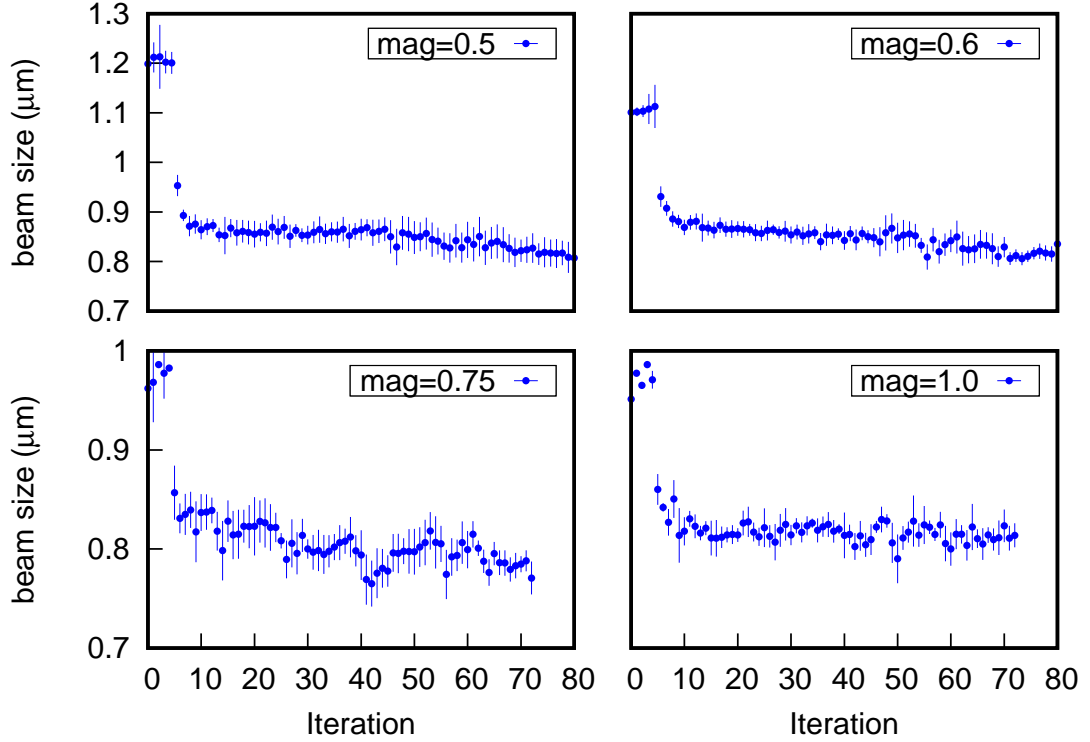
Figure 10: Optimized waist radius as a function of iteration steps. The initial waist radii are shown in Figure 8. Error bars represent one standard deviation of propagated fitting uncertainties.

The parameter N in the search algorithm is important because if N is too small, SLM might not be able to compensate for certain aberrations; but if N is too large, which means higher search space dimension, it takes longer time to complete the algorithm. $N = 10, 20, 36, 45$ and 91 have been tested by comparing their convergence after two full cycles. We found that when $N \geq 36$, the algorithm converges to same waist after two full cycles, which implies that Zernike term Z_i is much less significant for $i > 36$. $N = 10$ and 20 do not bring the waist down as much as $N = 36$; thus we keep $N = 36$ fixed for the rest of the discussions.
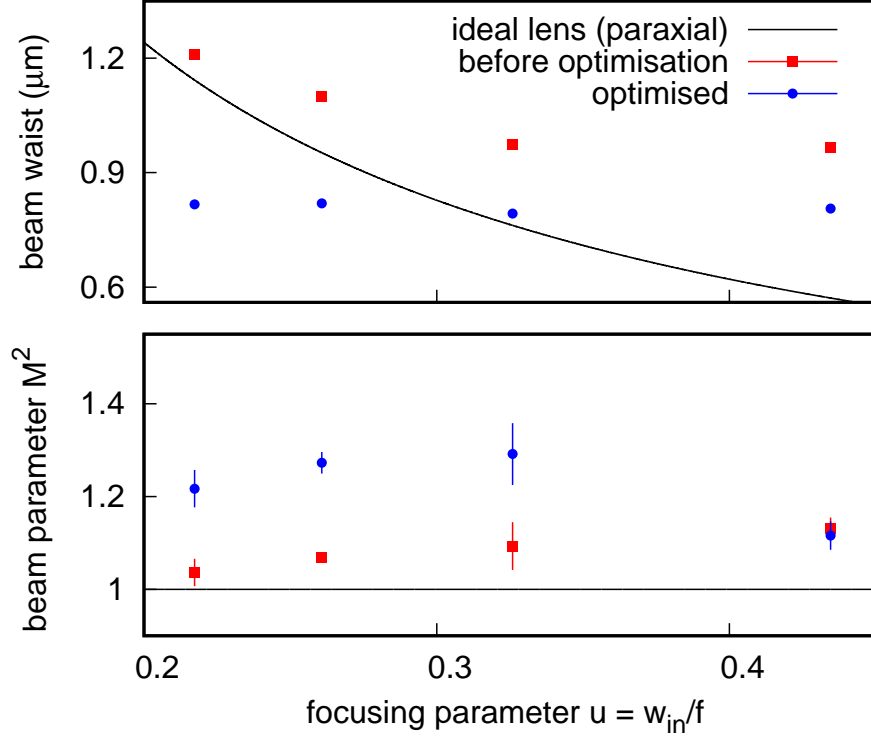
Figure 11: Waist radius and M^2 as a function of focusing parameter u. Black solid line: theoretical prediction for a paraxial ideal Gaussian beam. Red dots: data of beam waist when SLM performs as a flat mirror. Blue dots: data of beam waist at the end of waist optimization. Error bars represent one standard deviation of 10 repeated measurements. Error bars in top panel are smaller than symbol size.

4.4   Results and Discussions

Figure 10 demonstrates the results of gradient search optimization to minimize beam waist for different focusing parameter u. All of the four optimization runs follow the same trend; the waist radius reduces drastically within the first 10 iterations, then the improvement becomes quite moderate. The beam waist is close to convergence during the second cycle since the waist change is actually smaller than the fit error (iterations range between 37 and 72).

The characteristics of the corrected beam for different focusing parameter u are also illustrated by Figure 11. The beam waist decreases significantly in all
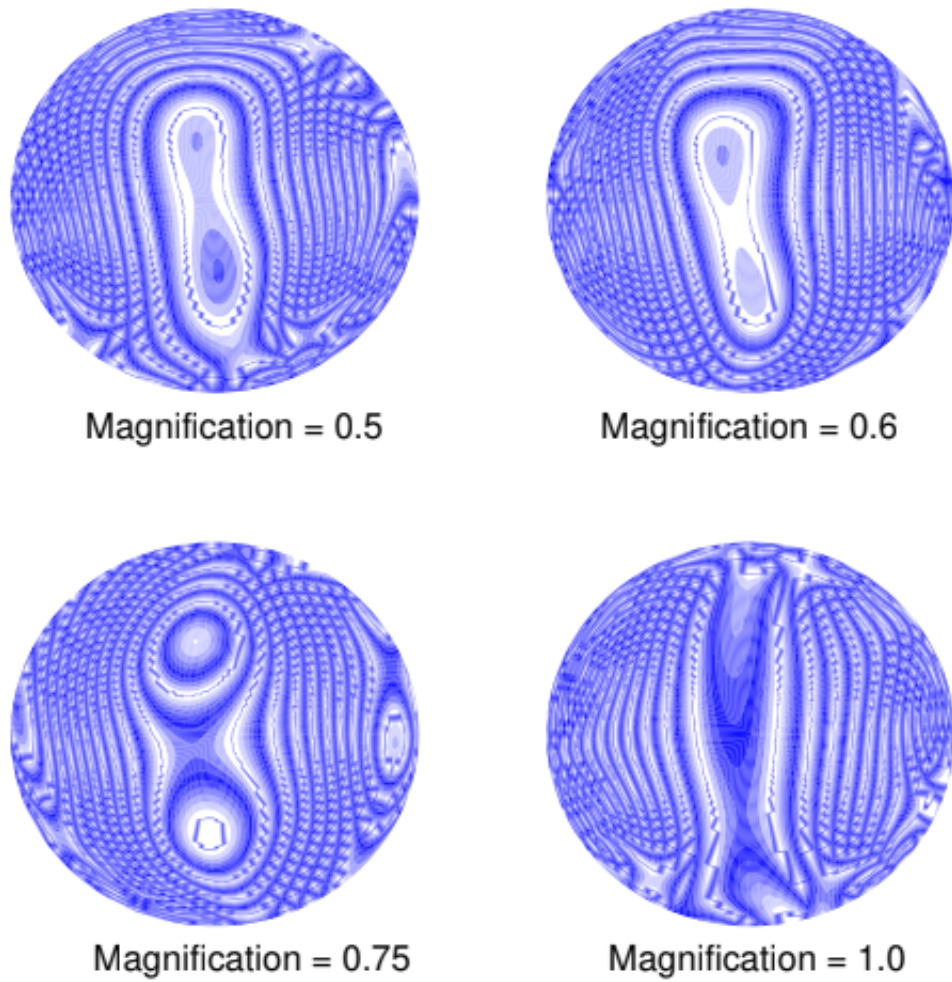
Figure 12: Contour plot of phase patterns that yield the smallest waist radius near focus at the end of optimization for different magnifications. The colour represents a phase of 0 (white) to π (blue).

of the four cases, which demonstrates improved focusing with the SLM. Here we observe two different optimization behaviours. For magnification 1.0 ($u = 0.435$), the beam waist reduces while maintaining its Gaussian profile (M^2 stays rather close to 1.0) . On the other hand, contrary to our expectation, in the case of small magnifications ($u = 0.217$ and $u = 0.261$), the algorithm does not solely apply wavefront correction for aberrations (which should yield optimized points near the black line). The scheme has actually managed to bring the waist radius of the first two points (magnification $= 0.5$ and 0.6) below the diffraction limit of a paraxial beam traversing ideal lens. The fairly large value of M^2 suggests that the SLM has actually deformed the Gaussian beam to achieve exaggeratedly small beam waist. The phase pattern applied onto the SLM for each focusing parameter u is plotted in Figure 12.

We want to confirm that the light intensity at the focal spot does increase at the end of optimization. Thus, the beam profile along x-direction is reconstructed from the discrete gradient of photodiode reading with respect to x-position of the razor near the focal point. Figure 13 shows the beam profile reconstructed for different magnifications. We observe approximately 30% improvement in light intensity for magnification $= 0.5$ and 0.6. For larger magnification, the improvement is less obvious.
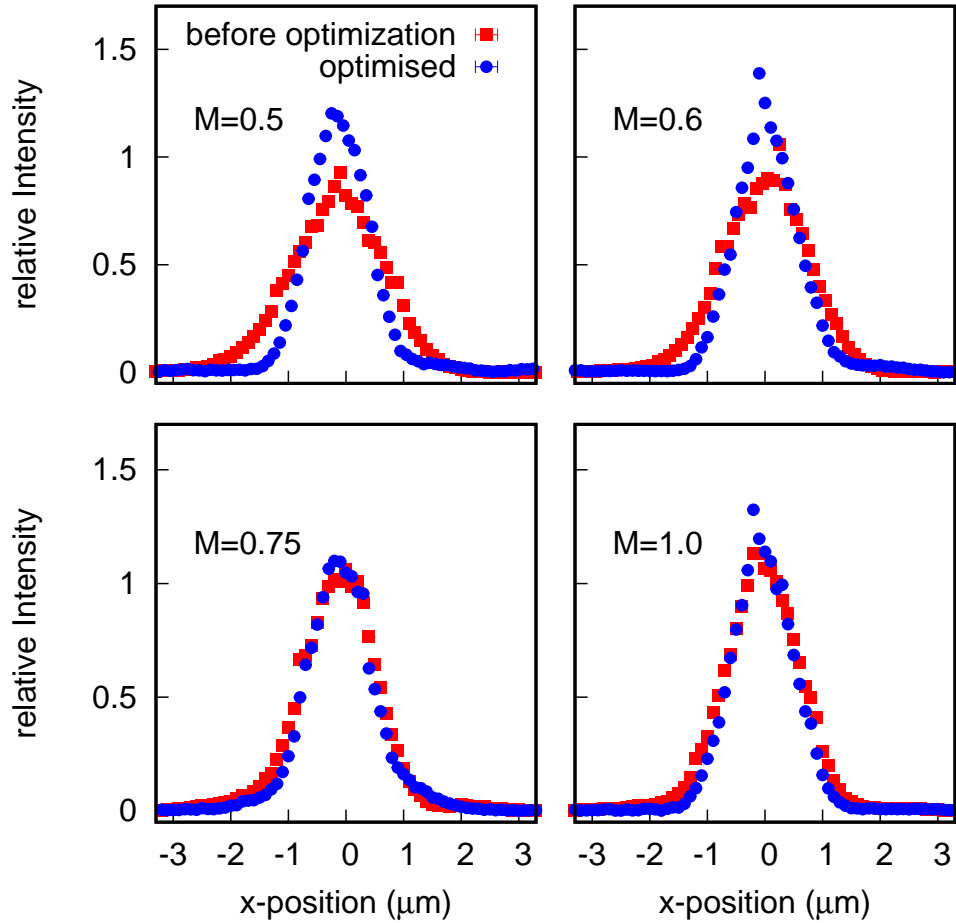
Figure 13: Beam profile reconstructed from the discrete gradient of photodiode reading. The intensity is normalized with respect to the peak of beam profile before optimization. Red dots: light intensity before the waist optimization. Blue dots: light intensity at the end of waist optimization.

5 Conclusion and Ongoing Work

We have demonstrated that focusing of laser beam can be improved using a SLM. The focal waist radius w_0 and beam parameter M^2 before and after the optimization are measured and compared. For small focusing parameters, the optimized beam waist radii are smaller than the theoretical predictions for a collimated Gaussian beam at the expense of having larger M^2. The intensity profile reconstructed shows 30% improvement in light intensity of the optimized light for small focusing parameters.

Currently, the waist radius is obtained from a single knife-edge cut across the beam along one direction. To maximize the light intensity at the focal point, we need to take into account both transverse directions on the focal plane. In the near future, we will implement a scheme that minimizes the focal spot size based on the waist radii along the two transverse directions using a SLM. Finally, we will extend the scheme to optimize atom-light interaction efficiency in the setup with trapped atoms.

References

[1] L.-M. Duan, M. D. Lukin, J. I. Cirac, and P. Zoller, "Long-distance quantum communication with atomic ensembles and linear optics," *Nature*, vol. 414, no. 6862, p. 413, 2001.

[2] P. W. H. Pinkse, T. Fischer, P. Maunz, and G. Rempe, "Trapping an atom with single photons," *Nature*, vol. 404, no. 6776, p. 365, 2000.

[3] S. Gleyzes, S. Kuhr, C. Guerlin, J. Bernu, S. Deleglise, U. B. Hoff, M. Brune, J.-M. Raimond, and S. Haroche, "Quantum jumps of light recording the birth and death of a photon in a cavity," *Nature*, vol. 446, no. 7133, p. 297, 2007.

[4] C. J. Hood, H. J. Kimble, and J. Ye, "Characterization of high-finesse mirrors: Loss, phase shifts, and mode structure in an optical cavity," *Phys. Rev. A*, vol. 64, no. 3, p. 33804, 2001.

[5] S. A. Aljunid, B. Chng, J. Lee, M. Paesold, G. Maslennikov, and C. Kurtsiefer, "Interaction of light with a single atom in the strong focusing regime," *J. Mod. Opt.*, vol. 58, no. 3-4, pp. 299–305, 2011.

[6] M. K. Tey, G. Maslennikov, T. C. Liew, S. A. Aljunid, F. Huber, B. Chng, Z. Chen, V. Scarani, and C. Kurtsiefer, "Interfacing light and single atoms with a lens," *New J. Phys.*, vol. 11, 2009.

[7] M. Sondermann, R. Maiwald, H. Konermann, N. Lindlein, U. Peschel, and G. Leuchs, "Design of a mode converter for efficient light-atom coupling in free space," *Appl. Phys. B*, vol. 89, no. 4, pp. 489–492, 2007.

[8] G. Zumofen, N. M. Mojarad, V. Sandoghdar, and M. Agio, "Perfect reflection of light by an oscillating dipole," *Phys. Rev. Lett.*, vol. 101, no. 18, pp. 1–4, 2008.

[9] D. J. Wineland, W. M. Itano, and J. C. Bergquist, "Absorption spectroscopy at the limit: detection of a single atom," *Opt. Lett.*, vol. 12, no. 6, p. 389, 1987.

[10] G. Wrigge, I. Gerhardt, J. Hwang, G. Zumofen, and V. Sandoghdar, "Efficient coupling of photons to a single molecule and the observation of its resonance fluorescence," *Nat. Phys.*, vol. 4, no. 1, p. 60, 2008.

[11] A. N. Vamivakas, M. Atatüre, J. Dreiser, S. T. Yilmaz, A. Badolato, A. K. Swan, B. B. Goldberg, A. Imamolu, and M. S. Ünlü, "Strong extinction of a far-field laser beam by a single quantum dot," *Nano Lett.*, vol. 7, no. 9, pp. 2892–2896, 2007.

[12] Y. S. Chin, M. Steiner, and C. Kurtsiefer, "Nonlinear photon-atom coupling with 4Pi microscopy," *Nat. Commun.*, vol. 8, no. 1, pp. 1–13, 2017.

[13] M. Fischer, M. Bader, R. Maiwald, A. Golla, M. Sondermann, and G. Leuchs, "Efficient saturation of an ion in free space," *Appl. Phys. B Lasers Opt.*, vol. 117, no. 3, pp. 797–801, 2014.

[14] L. Alber, M. Fischer, M. Bader, K. Mantel, M. Sondermann, and G. Leuchs, "Focusing characteristics of a 4 π parabolic mirror light-matter interface," *J. Eur. Opt. Soc.*, vol. 13, no. 1, pp. 1–8, 2017.

[15] M. K. Tey, Z. Chen, S. A. Aljunid, B. Chng, F. Huber, G. Maslennikov, and C. Kurtsiefer, "Strong interaction between light and a single trapped atom without the need for a cavity," *Nat. Phys.*, vol. 4, no. 12, pp. 924–927, 2008.

[16] Y. S. Chin, M. Steiner, and C. Kurtsiefer, "Quantifying the role of thermal motion in free-space light-atom interaction," *Phys. Rev. A*, vol. 95, no. 4, pp. 3–7, 2017.

[17] S. Quabis, R. Dorn, M. Eberler, O. Glöckl, and G. Leuchs, "Focusing light to a tighter spot," *Opt. Commun.*, vol. 179, no. 1, pp. 1–7, 2000.

[18] M. B. Schneider and W. W. Webb, "Measurement of submicron laser beam radii," *Appl. Opt.*, vol. 20, no. 8, p. 1382, 1981.

[19] R. L. McCally, "Measurement of Gaussian beam parameters," *Appl. Opt.*, vol. 23, no. 14, p. 2227, 1984.

[20] J. J. Chapmana, B. G. Norton, E. W. Streed, and D. Kielpinski, "An automated submicron beam profiler for characterization of high numerical aperture optics," *Rev. Sci. Instrum.*, vol. 79, no. 9, 2008.

[21] A. D. Hill, D. Hervas, J. Nash, M. Graham, A. Burgers, U. Paudel, D. Steel, C. Schneider, M. Kamp, S. Höfling, J. Wang, J. Lin, W. Zhao, and P. G. Kwiat, "Optimizing single-mode collection from pointlike sources of single photons with adaptive optics," *Opt. Express*, vol. 25, no. 16, p. 18629, 2017.

[22] J. A. Carpenter and T. D. Wilkinson, "Aberration correction in Spatial Light Modulator based mode multiplexers," *Opt. Fiber Commun. Conf. Fiber Opt. Eng. Conf. 2013*, no. c, p. JW2A.27, 2013.